Thickness dependent structural, electrical and optical properties of nanostructured zinc oxide thin films deposited by chemical spray technique

A. U. UBALE*, V. P. DESHPANDE
Thin Film Physics Laboratory, Department of Physics, Govt. Vidarbha Institute of Science and Humanities, Amravati 444 604, Maharashtra, India

Nanostructured thin films have attracted the attention of an increasing number of researchers from several disciplines in the last ten years due to their outstanding electronic and optical properties and due to their extensively useful applications in various optoelectronic devices. The structural, electrical and optical properties of the nanostructured ZnO thin films deposited by spray pyrolysis were investigated. The film structure and surface morphology was characterized by XRD and SEM analysis respectively. The optical properties of the film were highly affected by the smaller grain size of the material. In this study, the variation of the band gap (3.52 to 2.98 eV) and activation energy (0.5 to 0.27 eV) is represented as a function of the film thickness (86 to 235 nm). Effect of film thickness on H_2S gas sensitivity was also studied.

(Received February 7, 2011; accepted February 17, 2011)

Keywords: Thin films, Nanostructures, Chemical synthesis, Electrical properties, Optical properties

1. Introduction

In recent years, many conductive oxides have investigated immensely due to their wide range of applications in semiconductor devices particularly in gas sensing area. Zinc oxide is the most popular, profitable and promising member of the oxide family due to its attractive electrical, optical and piezoelectric properties [1-3]. In addition, it possesses many interesting other properties, such as a wide energy band-gap, large photoconductivity, and high excitonic binding energy [4-6]. high-quality nanostructured ZnO films are widely used in various fields such as light emitting diodes [7-9], photodetectors [10], laser diodes [11], gas sensors [12,13], field emission [14], and solar cells [15,16]. Nanomaterials have received much attention by worldwide material scientists for their uncommon properties compared to bulk phase in the last 10 years. Great efforts have taken for the synthesis of metal oxides with various nanostructures for their wide application [17-22]. ZnO nanostructures have been synthesized by many methods such as chemical vapour deposition [23], r.f. magnetron sputtering [24], reactive magnetron sputtering [25], CVD [26], sol-gel process [27], laser ablation [28] and spray pyrolysis [29] using different precursors [30-33]. Ahmad et al. [34] have synthesized uniform zinc oxide nanoparticles of about ~55 nm in diameter by the thermal decomposition of zinc compound. Out of these techniques, spray pyrolysis has many advantages such as simplicity, safety and cost affordability of equipment and raw materials. In this paper, we present the deposition of nanocrystalline ZnO thin films using spray pyrolysis method. The chemical reactants are selected such that the products other than the desired compound are volatile at the temperature of deposition. An appropriate choice of the precursor solution as well as the spray conditions can lead to high quality film deposition. This is easy, low cost and versatile technique, which is a potentially useful technique for large area deposition. The size dependent structural, optical, morphological, electrical and H_2S gas sensing properties of the films were studied by X- ray diffraction, optical absorption, scanning electron microscopy and electric measurements.

2. Experimental details

The spray system used for present work has vertical assembly that consists of spray nozzle, substrate heater, temperature controller and air compressor. To measure flow of precursor solution and air, liquid and gas flow meters are used. The horizontal motion of spray nozzle was controlled by stepping motor along with programmed microcontroller. The distance between spray nozzle and substrate heater was kept 25 cm. The film formation depends on the process of droplet landing, reaction and solvent evaporation, which are related to droplet size and momentum [35, 36]. The spraying solution was of 0.1 M zinc acetate dehydrate ($Zn(CH_3COO)_2, 2H_2O$) in distilled water. The solution was sprayed onto hot glass substrates using compressed air as a carrier gas. Several trials were conducted to optimize the different deposition parameters such as substrate temperature, spray rate, concentration of zinc acetate. All these optimized preparative parameters are discussed somewhere else [37]. The volume of zinc acetate solution was varied to obtain the films of different thickness. The average thickness of the film was measured

by the gravimetric and Fizzau's method. The two-point dc probe method of dark electrical resistivity was used to study the variation of resistivity with temperature. A copper block was used as a sample holder and chromel–alumel thermocouple was used to measure the temperature. For the measurement of resistivity, a constant voltage was applied across the sample and the current was noted using a digital nanometer. To study H_2S sensing behaviour ZnO resistance is measured in presence and in absence of gas as a function of temperature. The steady-state resistance were investigated in the temperature range 315 -381 K in dry air and 800 ppm H_2S in air. The structural studies were carried out using Philips PW 1710 diffractometer, with Cu-Ka radiation of 1.5405 A^0. The optical characteristics were studied using Hitachi 330 spectrophotometer to find band gap energy. The surface morphological studies were carried out using JSM-6360 scanning electron microscope.

3. Result and discussion

3.1. Film deposition

The aqueous solution of zinc acetate was sprayed on to glass substrate kept at 573 K. The thermal decomposition of zinc acetate took place at the substrate to give zinc oxide as,

$$Zn(CH_3OO)_2+H_2O \rightarrow ZnO + 2CH_3COOH\ (gas) \quad (1)$$

The atomization of the solution into a spray of fine droplets was carried out by the spray nozzle with the help of compressed air as carrier gas. During the course of the spray, the substrate temperature was monitored using a chromel alumel thermocouple, and was kept constant at 573 + 5K. By increasing the substrate temperature, the crystallization is enhanced due to complete thermal decomposition of zinc salt and the reactions at substrate surface are accelerated. In the present work, it is observed that films deposited at temperature less than 573 + 5K are powdery; it may be a result of incomplete thermal decomposition of zinc salt. The films of different thickness were prepared by varying the volume of spray solution as given in Table 1.

Table 1. Variation of ZnO film thickness (nm) with spray volume of zinc acetate (mL).

Sr. No.	Spray volume of 0.1 M zinc acetate (mL)	ZnO film thickness (nm)
1	8	86
2	12	123
3	16	175
4	20	199
5	24	235

3.2. Structural analysis

The structural properties of films were investigated by X-ray diffraction technique. Fig. 1 shows the X-ray diffraction spectra of ZnO films of different thickness. By comparison of observed and standard data (Table 2), it is concluded that the resulting compound is ZnO with hexagonal wurtzite type of crystal structure. The film having thickness of 86 nm shows amorphous nature; however, the crystallinity of ZnO increases with film thickness. As thickness increases, the (100) and (101) diffraction peaks become progressively more dominant along with the other peaks- (002) and (102). The average grain size of crystallites was calculated by using Scherrer formula [38],

$$d = \frac{\lambda}{\beta\cos\theta} \quad , \quad (2)$$

where λ is the wavelength used (0.154nm); β is the angular line width at half maximum intensity; θ is the Bragg's angle. The variation of grain size from 19 to 34 nm was observed with film thickness as shown in Fig. 2. Increase in the crystallization was observed from XRD peak of higher thickness film and this may be the possible reason for larger grains.

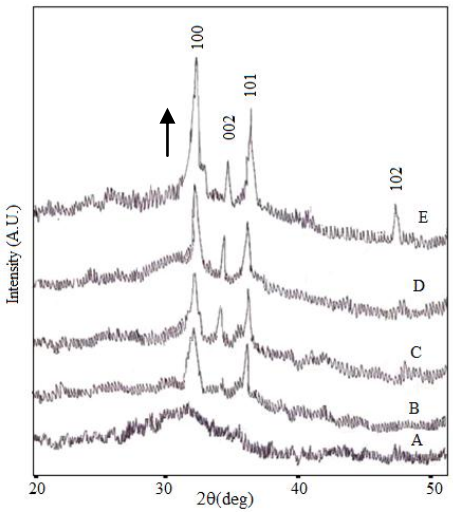

Fig. 1. XRD patterns of ZnO thin Films having thickness: (A) 86 nm; (B) 123 nm; (C) 175 nm; (D) 199 nm;(E)235nm.

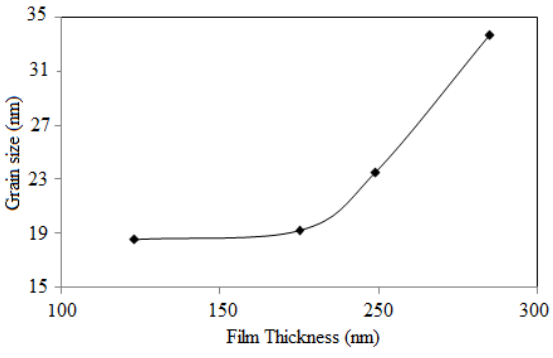

Fig. 2. Variation of grain size with thickness of ZnO thin film.

Table 2. Comparison of observed crystallographic data of ZnO thin film with standard JCPDS (79-0208) card.

Film thickness (nm)	h k l	Standard data		Observed data	
		2θ (degree)	d (A^0)	2θ (degree)	d (A^0)
86	-	-	-	-	-
123	100	31.619	2.827	31.681	2.821
	101	36.100	2.486	36.093	2.479
175	100	31.619	2.827	31.686	2.824
	002	34.335	2.609	34.320	2.619
	101	36.100	2.486	36.161	2.492
199	100	31.619	2.827	31.798	2.814
	002	34.335	2.609	34.238	2.619
	101	36.100	2.486	36.122	2.473
235	100	31.619	2.827	31.709	2.814
	002	34.335	2.609	34.361	2.609
	101	36.100	2.486	36.079	2.489
	102	47.367	1.917	47.345	1.920

3.3. Morphology

The SEM micrographs of ZnO films having different thickness are shown in Fig. 3. From micrographs, it is observed that the films are continuous with irregular distribution of grains. In addition, the grain growth is observed with thickness. The grains are slightly irregular and rod-shaped. With increase in thickness, the texture of the films is changed from relatively smooth porous network into a rough granular film. At low thickness a porous network contains large voids; however at higher thickness voids are disappeared and irregular growth is observed. The typical EDAX spectra of ZnO thin film of thickness 199 nm is shown in the Fig. 4. The peak at 0.525 KeV is from oxygen and the peaks at 0.99, 8.63, and 9.58 KeV are due to Zn respectively, which confirms the formation of ZnO.

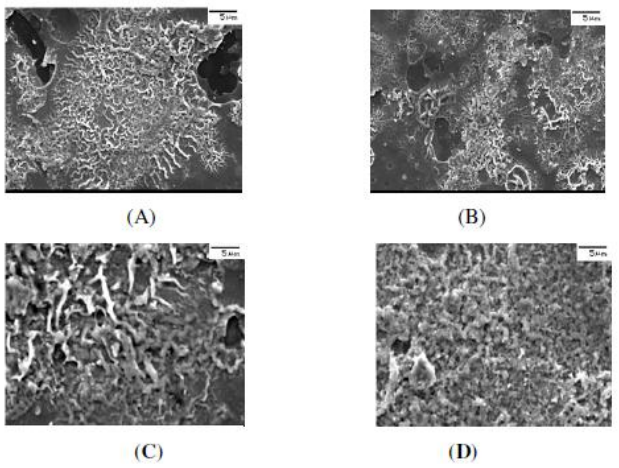

Fig. 3. SEM micrograph of ZnO thin film of thickness (A) 86 nm, (B)123 nm, (C) 175 nm., (D) 199 nm.

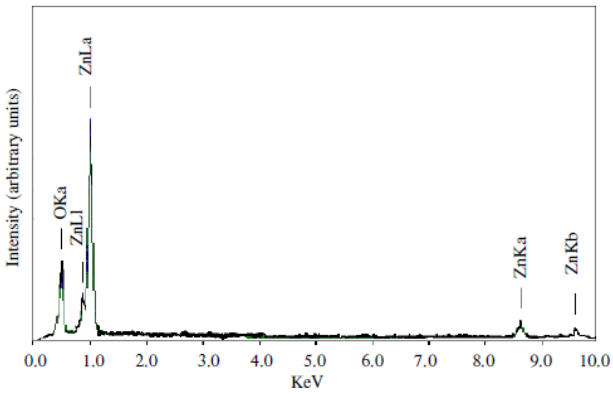

Fig. 4. Typical EDAX spectra of ZnO thin film of thickness 199 nm.

3.4. Optical analysis

The optical absorption in ZnO thin films of different thicknesses was studied in the wavelength range of 240 to 800 nm. Fig. 5 shows optical absorption curves for ZnO films with different thickness. The nature of transition is determined by using the relation,

$$\alpha = \frac{A(h\upsilon - Eg)^n}{h\nu}, \qquad (3)$$

where hν is the photon energy, E_g is the band gap energy, A and n are constants. For allowed direct transitions n = 1/2 for allowed indirect transitions n = 2.

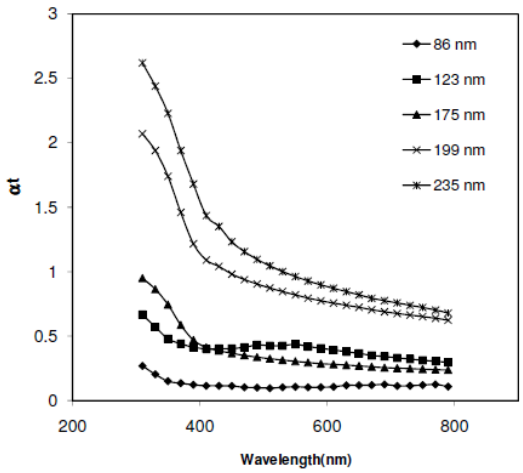

Fig. 5. Plot of optical absorption (αt) versus wavelength (nm) of ZnO thin films.

The width of the energy gap is a characteristic value for each material. The plot of $(\alpha h\nu)^2$ versus hν is shown in Fig. 6. The nature of plots indicates the existence of direct transition. With the help of slope, the band gap energy is calculated. As the thickness of the film increases, number of atoms increases growing from a single molecule to a macroscopic crystal. The previously distinct atomic orbitals overlap and form bands. The energy regions

between the highest possible energy of an electron in the valence band and the lowest possible energy of an electron in the conduction band are the forbidden energy gaps, where electrons are not allowed to exist quantum-mechanically in a crystal. The density of states can have very different shapes for different bands and levels. The energy of an electron in a band increases proportional to the square of its momentum relative to the band energy minimum in the k-space. The density of states in a band also depends on number of atoms and disorders in a nanostructured semiconductor that are more in nanosize thin films. Thus, they are strongly affected by the dimensions of the material. In present investigation, it is found that the band gap energy of ZnO decreases from 3.52 to 2.98 eV as the thickness varies from 86 to 235 nm (Fig. 7).

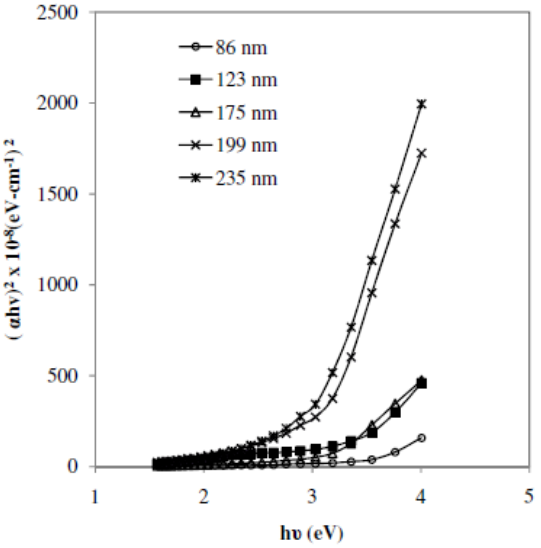

Fig. 6. Plots of $(\alpha h\nu)^2$ versus hν for ZnO films of different thicknesses.

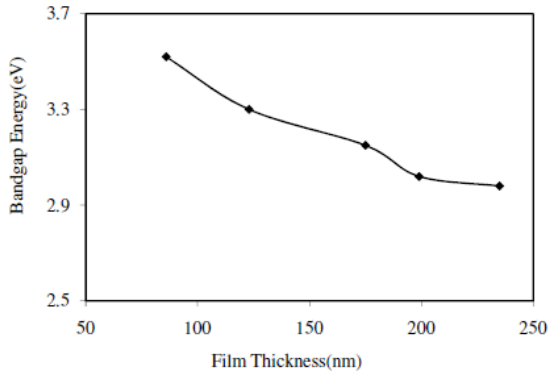

Fig. 7. Variation of optical band-gap energy Eg (eV) with ZnO film thickness.

3.5. Electrical analysis

Variation of DC-electrical resistivity with temperature was studied for ZnO film of different thickness. It was observed that, resistivity decreases as the film thickness increases. Also the decrease in the resistivity with increase in temperature is observed which shows that ZnO films are semiconducting. Fig. 8 shows variation of log (ρ) with reciprocal of temperature (1/T) for ZnO films of different thickness. The thermal activation energy was calculated using the relation,

$$\rho = \rho_0 \exp (E_0/KT), \quad (4)$$

where, ρ is resistivity at temperature T, ρ_0 is a constant; K is Boltzmann constant Activation energy was calculated from the graph of resistivity plots. Fig. 9 shows how resistivity of ZnO decreases with thickness at temperature 533 K. The change in resistivity and activation energy may be attributed to change in the density of free electrons and change in mechanism of scattering at the surface. In addition, in case of nanocrystalline materials, charge-transport is likely to be determined by potential barriers at the grain boundaries. Such barrier can decrease carrier mobility, and may also trap and release carriers to decrease carrier concentration, which decreases conductivity in nanosize ZnO thin films.

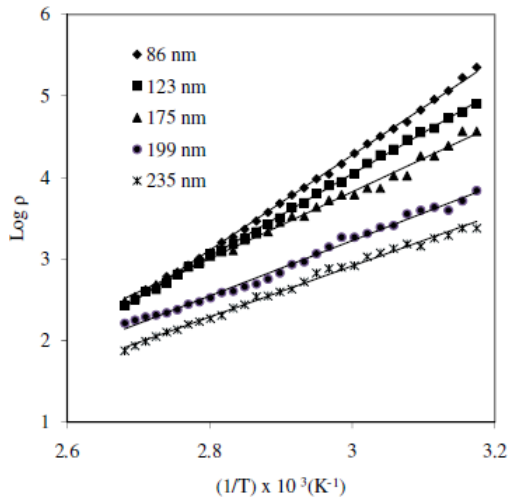

Fig. 8. Variation of log of electrical resistivity with (1/T) x 10^3 for of ZnO thin film.

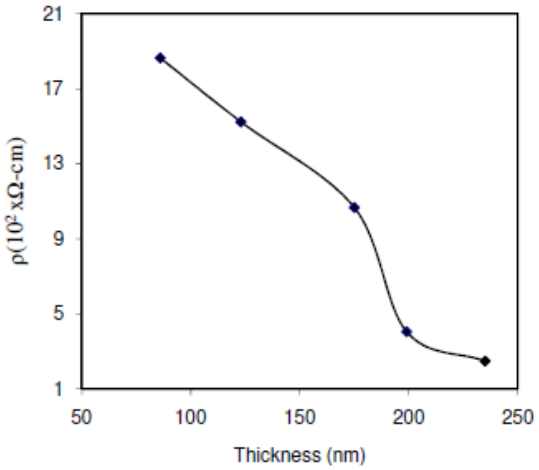

Fig. 9. Variation of electrical resistivity (ρ), with ZnO thin film thickness.

The variation of activation energy with film thickness is shown in Fig. 10. The activation energy decreases as the film thickness increases as the thicker films shows larger grains thus have fewer grain boundaries thus have higher mobility. Also thinner films are so porous and conduction path is not very continuous which also reduces mobility and conductivity.

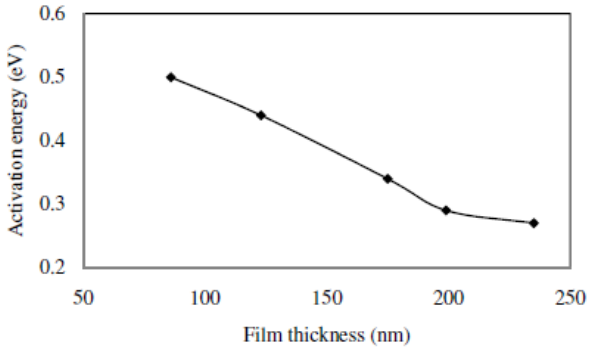

Fig. 10. Variation of activation energy with thickness of ZnO thin films.

3.6. H_2S gas sensing

As zinc oxide is electrically conductive and visually transparent, ZnO is a prime candidate in photovoltaic and gas sensor applications. ZnO is also chemically and mechanically stable against environmental corrosions [39]. The sensing properties of ZnO thin films were measured for H_2S gas. The sensitivity is measured by using the equation,

$$S = \frac{R_{air}}{R_{gas}} \quad , \qquad (5)$$

where, R_{gas} is resistance of the film in presence of H_2S gas, R_{air} is resistance of the film in absence of H_2S gas in air. Fig. 11 shows plots of sensitivity for ZnO thin films of various thicknesses. All the films show that the maximum sensitivity is at 360 K temperature. Measured H_2S gas-sensitivity of ZnO thin film of thickness 86 nm is less than the films of higher thickness. The gas sensitivity is more if crystallite provides larger surface area, altering the surface charge carriers or the electrical conduction between individual crystal grains at the gas absorption. In nanosize thin films, the grains are very small, naturally, they provide more surface area for absorption, but there is always possibility of some gaps between the grains. The cluster or grain density is less giving a limited area for absorption, which gives less sensitivity. The maximum sensitivity for 800 ppm of H_2S is estimated to be 0.91 for ZnO film of thickness 86 nm and it increases to 4.16 for 175 nm thickness and again decreases to 3.46 for 235nm thickness. It supports that in ultra thin films the grains are very small with bigger voids. The film of thickness 175 nm shows more sensitivity as it provides maximum surface area.

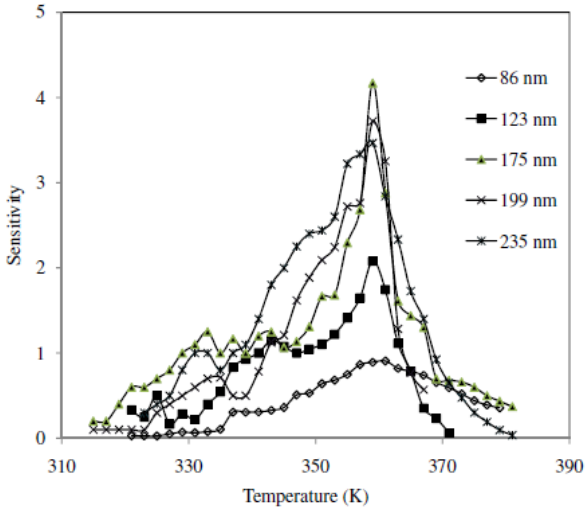

Fig. 11. Variation of H_2S gas sensitivity of ZnO thin films.

4. Conclusions

ZnO thin films of varying thickness were prepared using chemical spray pyrolysis technique. The structural, electrical and optical properties of nanostructured ZnO films were investigated. The XRD pattern suggests that the films are nanocrystalline in nature having hexagonal wurtzite type structure. SEM micrograph shows that the films are continuous with irregular distribution of grains. Analysis of UV/VIS spectra of the films reveals that the material is a direct semiconductor with the band gap in the range of 3.52 to 2.98 eV. The electrical resistivity and activation energy measurement shows thickness-dependent character. The H_2S sensing character of ZnO is also found as thickness-dependent.

Acknowledgement

The authors are thankful to University Grants Commission, WRO, Pune (India), for financial support under the project (No: F47-258/2007).

References

[1] A. Sanchez-Juarez, A. Tiburcio-Silver, A. Ortiz, Sol. Energy Mater. Sol. Cells, **52**, 301 (1998).
[2] F. Hamdani, D. J. Smith, H. Jang, W. Kim, A. Salvador, A. E. Botharev, J. M. Gibson, A. Y. Polyakov, M. Skowronski, H. Morkoc, J. Appl. Phys., **83**, 983 (1998).
[3] J. Hu, R. G. Gordon, J. Electrochem. Soc., **139**, 2014 (1992).
[4] K. H.ummer, Phys. Stat. Sol., **56**, 249 (1973).
[5] J. H. Lee, K. H. Ko, B. O. Park, J. Cryst. Growth, **247**, 119 (2003).
[6] B. Cao, W. Cai, Y. Li, F. Sun, L. Zhang, Nanotechnology, **16,** 1734 (2005).
[7] T. Aoki, Y. Hatanaka, D. C. Look, Appl. Phys. Lett., **76**, 3257 (2000).

[8] N. Saito, H. Haneda, T. Sekiguchi, N. Ohashi, I. Sakaguchi, K. Koumoto, Adv. Mater., **14**, 418 (2002).
[9] D. K. Hwang, S. H. Kang, J. H. Lim, E. J. Yang, J. Y. Oh, J. H. Yang, S. J. Park, Appl. Phys. Lett. **86**, 222101 (2005).
[10] Y. Liu, C. R. Gorla, S. Liang, N. Emanetoglu, Y. Lu, H. Shen, M. Wraback, J. Electron. Mater., **29**, 69 (2000).
[11] D. C. Reynolds, D. C. Look, B. Jogai, Solid State Commun., **99**, 873 (1996).
[12] V. R. Shinde, T. P. Gujar, C. D. Lokhande, Sens. Actuators B: Chem., **123**, 701 (2007).
[13] J. Xu, Q. Pan, Y. Shun, Sens. Actuator, **B 66,** 277 (2000).
[14] K. Vanheusden, C. H. Saeger, W. L. Warren, D. R. Tallant, J. A. Voight, Appl. Phys. Lett. **68**, 403 (1996).
[15] K. Westermark, H. Rensmo, T. A. C. Lees, J. G. Vos H. T. Siegbahn, J. Phys. Chem. **B 10**, 10108 (2002).
[16] N. Golego, S. A. Studenikin, M. Cocivera, J. Electrochem. Soc., **147**, 1592 (2000).
[17] K. Woo, H. J. Lee, J. Ahn, Y. S. Park, Adv. Mater., **15**, 1761 (2003).
[18] K. Nakaoka, J. Ueyama, K. Ogura, J. Elect. Chem., **571**, 93 (2004).
[19] J. B. Reitz, E. I. Solomon, J. Am. Chem. Soc., **120**, 11467 (1998).
[20] Y. Joseph, W. Ranke, W. Weiss, J. Phys. Chem., **B 104**, 3224 (2000).
[21] L. Vayssieres, Adv. Mater. **15**, 464 (2003).
[22] M. M. Thackeray, Prog. Solid State Chem., **25**, 1 (1997).
[23] B. Cheng, E. T. Samulski, Chem. Commun., **8**, 986 (2004).
[24] Z. Y. Fan, D. W. Wang, P. C. Chang, W. Y. Tseng, J. G. Lu, Appl. Phys. Lett., **85**, 5923 (2004).
[25] Z. C. Jin, I. H. Amberg, C. G. Granquist, J. Appl. Phys., **64**, 5117 (1988).
[26] O. F. Khan, P. O Brien, Thin Solid Films, **173**, 95 (1989).
[27] Y. Ohya, H. Saiki, J. Mater. Sci., **29**, 4099 (1994).
[28] Z. Y. Ning. S. H. Cheng, S. B. Ge, Y. Chao, Z. Q. Gang, Y. X. Zhang, Z. G. Lin. Thin Solid films, **307**, 50 (1997).
[29] S. Major, A. Banerjee, K. L. Chopra, Thin Solid Films, **108**, 333 (1983).
[30] B. D. Cullity, S. R. Stock. Elements of X-Ray diffraction. Preventice Hall (2001).
[31] Y. C. Zhang, X. Wu, X. Y. Hu, R. Guo, J. Cryst. Growth, **280**, 250 (2005).
[32] Y. J. Xing, Z. H. Xi, Z. Q. Xue, X. D. Zhang, J. H. Song, R. M. Wang, J. Xu, Y. Song, S. L. Zhang, D. P. Yua, Appl. Phys. Lett., **83**, 1689 (2003).
[33] J. X. Duan, X. T. Huang, E. K. Wang, H. H. Ai, Nanotechnology, **17**, 1786 (2006).
[34] T. Ahmad, S. Vaidya, N. Sarkar, S. Ghosh, A. K. Ganguli, Nanotechnology, **17**, 1236 (2006).
[35] C. M. Lampkin, Prog. Cryst. Growth Charact., **1,** 406 (1979).
[36] P. S. Patil, Mater. Chem. Phys., **59**, 185 (1999).
[37] A. U. Ubale, S. C. Shirbhate, J. Alloys Comp., **500**, 138 (2010).
[38] S. Major, A. Banerjee, K. L. Chopra, Thin Solid Films, **143**, 19 (1986).
[39] P. Samarasekara, N. U. S. Yapa, N. T. R. N. Kumara M. V. K. Perera. Bull. Mater. Sci., **30**, 113 (2007).

*Corresponding author: ashokuu@yahoo.com